Effectiveness of Foam Structures for Meteoroid Protection

S. J. PIPITONE* AND B. W. REYNOLDS†
Goodyear Aerospace Corporation, Akron, Ohio

Several meteoroid protection systems have been analyzed and tested for use in rigid or foldable space or lunar structures. This paper deals with double-wall systems in which a thin outer wall and a foam spacer are attached to an inner structural wall. The foam spacer serves as a mechanical atmosphere, tending to absorb and arrest impacting materials. Foam has exhibited an efficiency, by weight, 15.7 times that provided by a single aluminum alloy wall. Test results are presented, and hypotheses explaining phenomena encountered are suggested. Significant trends in materials and techniques for protection from hypervelocity impacts are exhibited.

Introduction

As part of a program for evaluating space and lunar structures made of both rigid and flexible materials, Goodyear Aerospace Corporation has experimentally and theoretically investigated hypervelocity terminal effects.

An initial literature review indicated that multiple-wall structures would prove effective. It was also found that many types of materials were, for the most part, being neglected. Therefore, a program of experimentation was initiated to compare the meteoroid penetration resistance of polymeric materials with that of aluminum materials and thereby to determine the significance and general order of importance of the various materials and experimental parameters. The primary objective was to provide data that would be useful in future space vehicle design.

Two basic types of damage are expected from meteoroid impacts:

1) Smaller (micrometeoroid) particles striking the outer wall of a space structure tend to erode the surface, causing changes in the optical properties and subsequently affecting the thermal balance of the structure.

2) Larger meteoroid particles may penetrate the space structure and cause spalling, accompanied by or independent of penetration.

Impacts by larger meteoroids could produce other types of damage to a space structure, such as structural failure, loss of internal pressurizing and life-supporting gases, equipment damage, explosive decompression, and catastrophic atmospheric flash.[1] This paper is limited to exterior meteoroid protection and is directed toward work done in the development of a protection system that precludes damage to the structural or load-carrying wall, whether rigid or flexible materials are selected for a given structure. The use of other safety and repair methods against meteoroid penetration of the structural wall would naturally be part of a space vehicle design. Partitioning, leak detection, and repair are several other methods of decreasing the meteoroid penetration hazard which would be incorporated along with the exterior protection into a composite space vehicle protection system.

Meteoroid Environment

The design of an efficient meteoroid protection system involves an understanding of both the meteoroid environment and the hypervelocity impact phenomena. Although progress is being made, the present technology level in both areas contains important uncertainties. A review in depth of these problems is beyond the scope of this paper; details can be found in the references.

Meteoroid flux, mass, composition, velocity, and spatial position are the significant environmental factors in protection system design. Figure 1 summarizes meteoroid flux and mass determinations. Unfortunately, data are lacking in the mass regime where the greatest penetration hazard is indicated. A conservative and simple function relationship[2] was tentatively selected for the preliminary design of vehicles proposed for close-earth orbits. This relationship is defined by

$$F_{>} = 1 \times 10^{-14}\, m^{-1.38} \qquad (1)$$

where $F_{>}$ is the number of particles per square meter-second of mass greater than or equal to m in grams.

Meteoroids have been classified in three groups by density. Ninety percent of the total flux $F_{>}$ consists of particles with a density of 0.5 g/cm³: 9% consists of particles with a density of 2.8 g/cm³, and 1% consists of particles with a density of 7.8 g/cm³. The low density particles, 0.5 g/cm³, are believed to be higher density particles held together by fragile, porous matrix materials.[3–5]

Meteoroid velocity is believed to decrease as the particle mass decreases. This relationship is shown in Fig. 2. The average meteoroid presenting a perforation hazard to vehicles in a near-earth orbit is believed to have a relative velocity of no less than 50,000 fps.[5]

Meteoroid Simulation Facilities

Until recently, with the exception of a few scattered points the maximum impact velocity achievable in the laboratory for projectiles of known mass appeared to be 12,000 fps. Early in 1962, several simulation facilities were found capable of accelerating small spherical projectiles weighing from 1 to 10^{-4} g to velocities approaching 24,000 fps by using light-gas guns. By the end of the year there were several facilities capable of accelerating particles to 50,000 fps and above, by use of exploding-foil techniques. Various shaped-charge devices have been used to accelerate particles to and above 30,000 fps. Such facilities require ingenious instrumentation for measuring particle mass just before impact. If acceleration techniques continue to be improved at the present pace, adequate simulation of meteoroid particle sizes and velocities will be attained in the near future.[2]

Although considerable work still is required in the area of measuring and recording phenomena associated with hyper-

Presented as Preprint 2895-63 at the AIAA Launch and Space Vehicle Shell Structures Conference, Palm Springs, Calif., April 1–3, 1963; revision received October 31, 1963.

* Manager, Space Systems Division. Member AIAA.

† Development Engineer, Aeromechanics Technology Division. Member AIAA.

velocity impact, several techniques have proved useful for velocity measurement. High-speed photography permits submicrosecond observation of surface phenomena at impact and of such interior behavior as crater enlargement, shock propagation, and fracture (in transparent targets). Flash x-ray photography has made possible close study of transient density changes, as well as surface and interior processes. Pressure-time profiles have been obtained during crater formation. Impulse measurement by ballistic pendulum techniques, recovery of particle fragments and residue, and recovery of spall particles is permitting more rigorous quantitative analysis. However, no single facility provides all the desirable techniques for complete qualitative and quantitative analyses of hypervelocity impact phenomena.[2]

Experimental Data

GAC hypervelocity firings were conducted by the Armour Research Foundation of Illinois Institute of Technology at Chicago. The projectiles used were 4.54-mg Pyrex and 4.95-mg steel spheres. Target specimens were designed on the basis of findings of other investigators. Funkhouser,[6] using 0.062-in. copper projectiles fired at velocities of 12,000 fps at double-wall, aluminum targets, concluded that 0.01- to 0.02-in. bumpers gave the best penetration protection and that bumper spacing beyond 2 in. is unwarranted. Nysmith and Summers,[7] using $\frac{1}{8}$-in. Pyrex projectiles fired at 11,000-fps velocities at multiple-wall aluminum targets, concluded that increasing the number of sheets, increasing the wall spacing, and using a spacer of lightweight filler material increases penetration resistance. Using these results, a hypothesized target-specimen design was formulated.

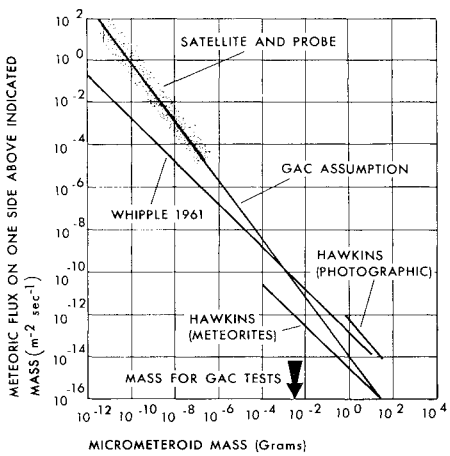

Fig. 1 Meteoroid flux in near-earth environment.

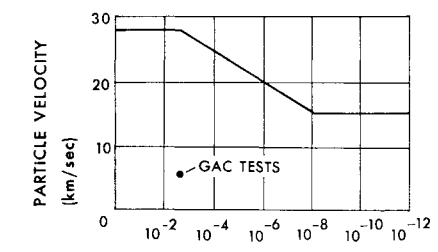

METEOROIDS

Density (g/cm^3)	Total flux (percent)
0.5	90
2.8	9
7.8	1

TEST PROJECTILES

Characteristic	Pyrex	Steel
Density (g/cm^3)	2.12	7.8
Diameter (in.)	0.063	0.042
Mass (mg)	4.54	4.95

Fig. 2 Meteoroid mass-velocity relationship.

The nomenclature used to describe specimen configuration is given in Fig. 3. Initially, the hypothetical specimen design for hypervelocity penetration resistance was conceived to function as follows. The bumper serves to fragment meteoroids having sufficient mass to cause penetration. The spacer positions the outer wall (or walls) and may arrest and absorb the shattered, impacting materials. The inner wall may be of a more economical design from the standpoint of weight and yet perform much the same function as the bumper, that is, to fragment and stop meteoroids. The structural wall carries the structural loads and serves as the

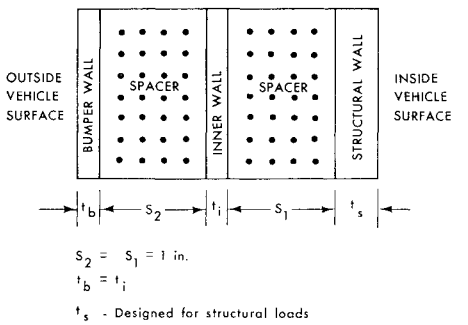

Fig. 3 Schematic of initial hypothetical specimen configuration (used for single-, double-, and triple-wall specimens).

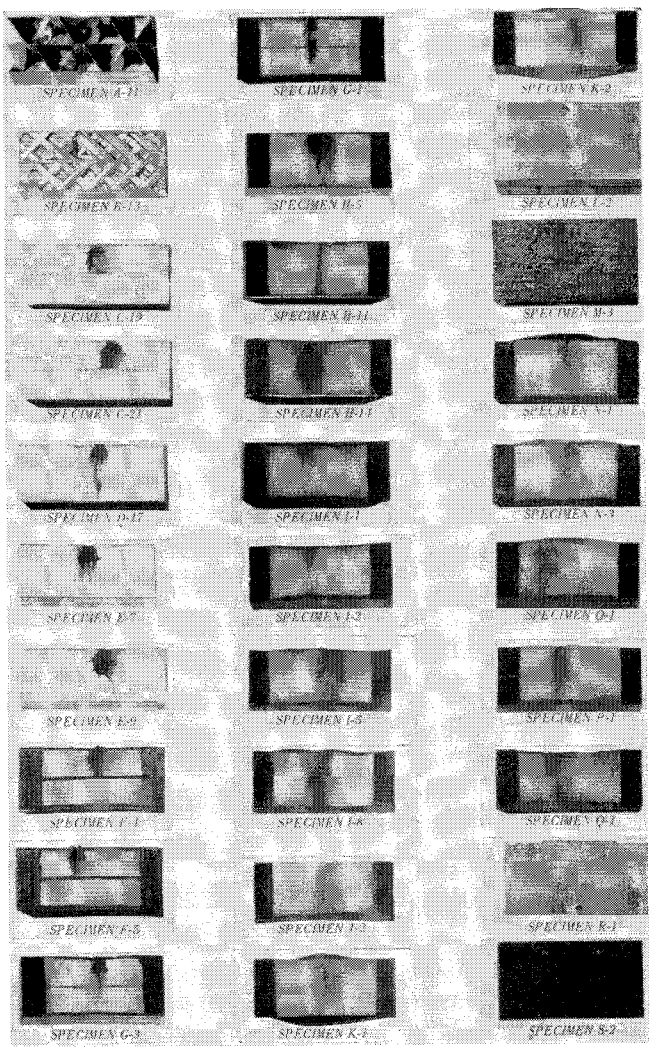

Fig. 4 Hypervelocity penetration specimens. Projectiles for all specimens except *H*-14 and *I*-8 were 0.063-in. Pyrex (4.54 mg). *H*-14 and *I*-8 were 0.042-in. steel (4.95 mg).

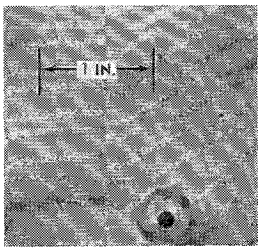

Aluminum bumper, specimen *E*-9

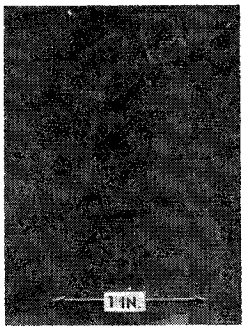

Polyurethane bumper, specimen *N*-3

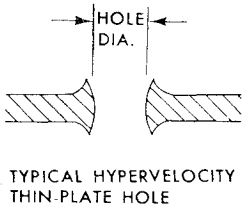

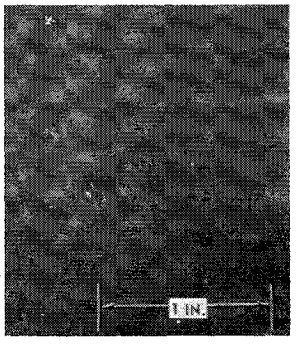

Mylar bumper, specimen *Q*-1

Fig. 5 Homogeneous bumper impacts.

gas-retaining wall for pressurized, manned space structures.

Impacted specimens are shown in Fig. 4. Specimens are identified by a letter and number; letters denote the construction and numbers designate individual specimens of a given construction.

Bumper and Structural Wall Test Results

Target specimens of varied bumper constructions were used so that data could be obtained on both homogeneous and composite (heterogeneous) materials with flexible and rigid characteristics.

Typical hypervelocity projectile impacts on homogeneous bumper materials are shown in Fig. 5. The homogeneous bumper materials demonstrate the typical lip formation characteristics of hypervelocity impacts in the fluid impact region, as is shown by the aluminum bumper specimen *E*-9. In addition, the polyurethane bumper *N*-3 reveals a sunburst pattern suggestive of stress lines about the circular hole; the Mylar bumper *Q*-1 shows minor radial cracks.

The typical hypervelocity thin plate hole is shown in cross section in Fig. 5. The outer lip formed on homogeneous bumpers consists of material raised above the original outside surface around the circular hole. Upon hypervelocity impact, a hemispherical crater initially is formed by the impact pressure. Subsequently, the particle and target materials flow along the surface of the expanding crater and are ejected in the opposite direction from that of the projectile. The final ejection of materials results in formation of this lip.

The inside surface of homogeneous bumpers exhibited lip formations as pronounced as the outer surface. The inside lip is probably attributable to the bumper material carried with the projectile during the final phase of pushing through the bumper.

The heterogeneous bumpers generally evidenced adhesion or delamination failure about the impact point (Fig. 6) with two exceptions: the René 41-CS-105 bumper *P*-1 exhibited minute radial cracks about a circular hole, and Dacron-Neoprene bumpers impacted at 12,800 fps had no noticeable defects. The adhesion and delamination failures can be attributed to the heat generated at impact and to ejection of minute fragments of bumper material immediately after impact. However, the adhesion or delamination failure area about the hole still should be partially effective in fragmenting any impacting meteoroid.

The *Z*-panel bumpers (*C*-21, Fig. 6) showed pronounced blow-back effects. *Z* panels are crushed aluminum honeycomb between two thin aluminum face sheets. The blow-back and the large area of damage associated with it can probably be explained as being the results of the mechanisms of crater growth.

Specimens *L*-2 and *M*-3, Fig. 7, were aluminum double-wall and Dacron-Neoprene double-wall specimens of equal weights but having no spacer mediums. The impact side of the structural wall of the aluminum specimen exhibited a series of concentric circular patterns of small pits that were most intense in and on a circle of 0.6-in. diam and diminished in intensity as the circles grew larger. The reverse side had a permanent set that corresponded to the intense pitting on the impact side. The impact side of the structural wall of the fabric specimen showed limited pitting and a change in texture inside a circle of 0.5-in. diam. No damage was visible on the reverse side.

Two single-wall specimens, *S*-2 (Dacron-Neoprene fabric) and *R*-1 (aluminum alloy), of equal weight were also impacted and sustained approximately equal damage. These single-wall penetrations show concisely the need for additional lightweight protection from the impacting projectile. That additional protection can be provided by foam-spacers with or without a bumper wall will be shown.

Spacer Test Results

The medium that positions the bumper, the interior wall, and the structural wall from one another is identified here

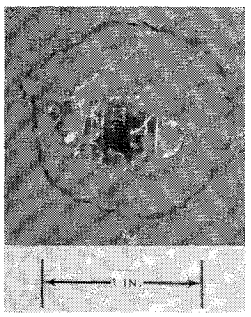

Aluminum honeycomb *Z* panel bumper, specimen *C*-21

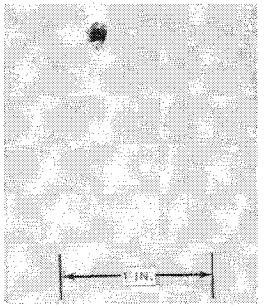

Fiberglass silicone bumper, specimen *K*-82

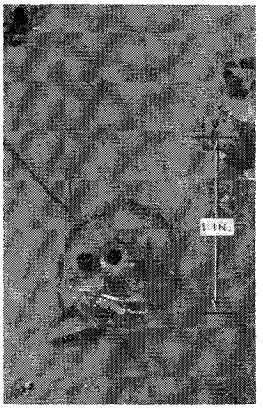

Mylar laminate bumper, specimen *O*-1

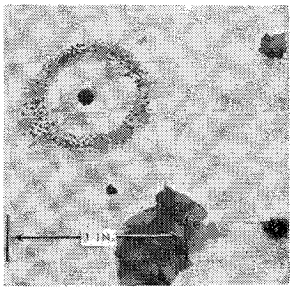

René 41- CS-105 number, specimen *P*-1

Fig. 6 Heterogeneous bumper impacts.

as a spacer. Depending on the spacer material, this medium provides additional protection for the structural wall. A foam spacer, for example, serves as a mechanical atmosphere that tends to absorb and arrest the impacting particles through vaporization. Under hypervelocity impact conditions this vaporization of the foam spacer causes cavities of various sizes and shapes to be formed. The size and shape of the cavities are functions of the bumper (material and mass), of the spacer (material and mass), and of the projectile (material, mass, density, and velocity) (see Fig. 4).

The aluminum sheet truss spacer of *A*-11 reveals widespread pitting and penetration. The aluminum sheet honeycomb trussgrid spacer *B*-13 shows twisted, torn, ellipsoidally shaped damage. The rigid 4-lb/ft^3 polyurethane foam-spacer cavities are displayed by *C*-21 and *E*-9. The triple-wall *Z*-panel specimen *C*-21 displays a cylindrical cavity with a slight indentation of the interior wall, but the 21-mil aluminum bumper specimen *E*-9 has a spheroidal cavity in the spacer medium.

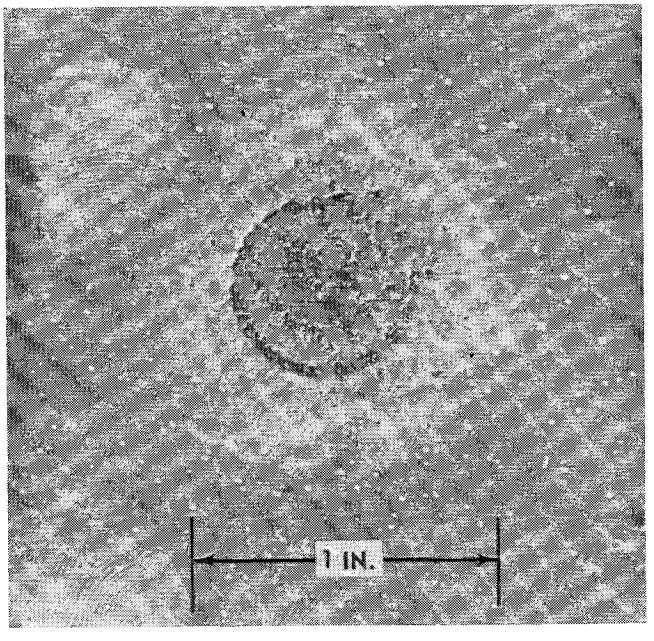

Structural wall impact, specimen *L*-2

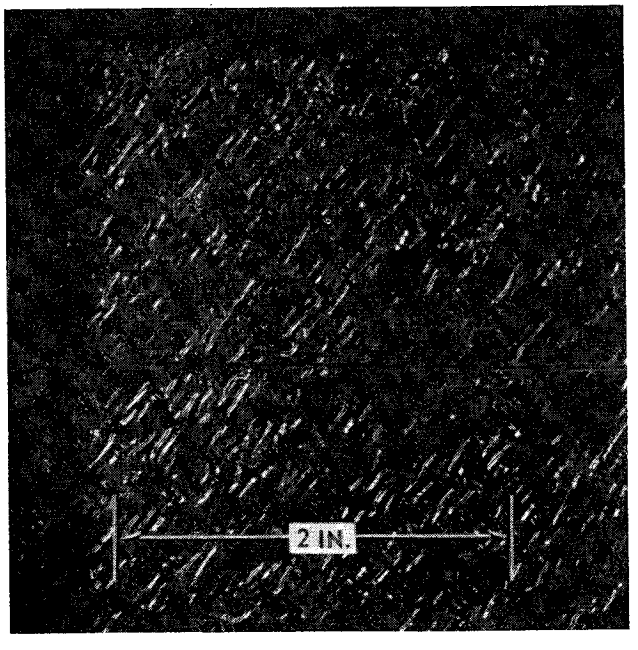

Structural wall impact, specimen *M*-3

Fig. 7 Structural wall damage when no spacer was used.

The lightweight 1.2 lb/ft^3 flexible, polyurethane foam spacers were tested using a variety of bumper materials. Two types of cavity formations were observed: ellipsoidal and cylindrical. Specimens *H*-5, *I*-5, *K*-1, *N*-3, *O*-1, and *P*-1 had ellipsoidal-shaped cavities. These specimens all had a 12 mil aluminum bumper (or its equivalent by weight).

Cylindrical cavities in the lightweight, flexible, polyurethane foam spacers were attributable to several different causes: 12,000 fps Pyrex projectiles, steel projectiles, 1-mil aluminized Mylar, and the absence of a bumper.

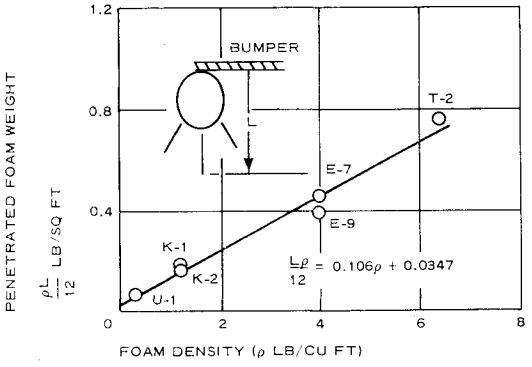

Fig. 8 Penetrated foam weight comparisons.

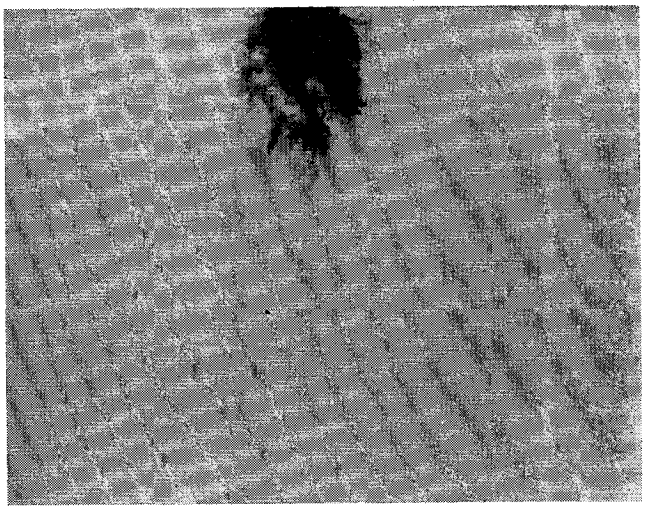

a) Specimen *T*-2

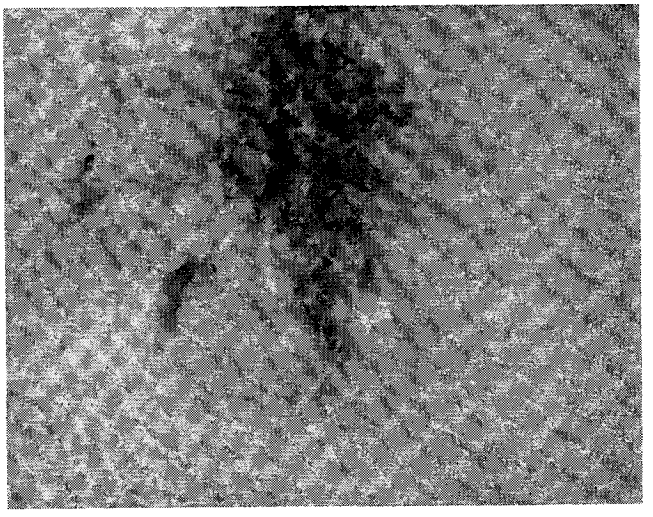

b) Specimen *U*-1

Fig. 9 Penetration test specimens *T*-2 and *U*-1: a) density 6.38 lb/ft^3, 0.00454-*GM* spherical projectile, velocity 19,100 fps; b) density 0.35 lb/ft^3, 0.00454-*GM* spherical projectile, velocity 20,200 fps.

Table 1 Weight of target specimens penetrated by 4.54 mg Pyrex projectiles of 0.063-in. diam

Specimen	Bumper wall		Spacer medium		Projectile velocity, 10^3 fps	Penetrated weight, lb/ft²				Penetration stopped by	
	Material	Weight, lb/ft²	Material	Weight, lb/ft²		Total	Outer wall	Foam	Interior wall	Spacer medium	Interior wall
J-2	none	...	polyurethane foam	1.2	21.9	0.20	...	0.20	...		*X*
Q-1	1-mil Mylar	0.01	polyurethane foam	1.2	21.3	0.21	0.01	0.20	...		*X*
K-1	fiberglass-silicone	0.17	polyurethane foam	1.2	21.3	0.33	0.17	0.16	...	*X*	
K-2	fiberglass-silicone	0.17	polyurethane foam	1.2	20.0	0.34	0.17	0.17	...	*X*	
N-1	polyurethane	0.16	polyurethane foam	1.2	19.3	0.36	0.16	0.20	...		*X*
P-1	René 41-CS-105	0.16	polyurethane foam	1.2	20.8	0.36	0.16	0.20	...		*X*
N-3	polyurethane	0.17	polyurethane foam	1.2	20.0	0.37	0.17	0.20	...		*X*
O-1	3-ply Mylar	0.17	polyurethane foam	1.2	22.25	0.37	0.17	0.20	...		*X*
H-5	aluminum 2024T3	0.17	polyurethane foam	1.2	21.4	0.37	0.17	0.20	...		*X*
I-5	Dacron-Neoprene	0.17	polyurethane foam	1.2	21.8	0.39	0.17	0.20	...		*X*
U-1	aluminum 2024T3	0.32	rigid polyurethane foam	0.35	20.2	0.39	0.32	0.07	...	*X*	
A-11	aluminum 2024T3	0.30	aluminum sheet truss	3.4	19.2	0.57	0.30	0.27	...		*X*
B-13	aluminum *Z* panel	0.31	aluminum honeycomb	4.2	19.1	0.66	0.31	0.35	...		*X*
L-2	aluminum 2024T3	0.17	none	...	20.5	0.71	0.17	..	0.54[a]		*X*
E-9	aluminum 2024T3	0.30	rigid polyurethane foam	4.0	20.8	0.72	0.30	0.42	...	*X*	
E-7	aluminum 2024T3	0.30	rigid polyurethane foam	4.0	19.1	0.75	0.30	0.45	...	*X*	
M-3	aluminum 2024T3	0.18	none	...	21.2	0.77	0.18	...	0.59[a]		*X*
F-4	Dacron-Butyl	0.42	flexible latex foam	6.0	19.5	0.90	0.42	0.48	...		*X*
F-5	Dacron-Butyl	0.42	flexible latex foam	6.0	18.85	0.90	0.42	0.48	...		*X*
D-17	aluminum *Z* panel	0.31	rigid polyurethane foam	4.0	19.05	0.92	0.31	0.61	...	*X*	
C-19	aluminum *Z* panel	0.31	rigid polyurethane foam	4.0	19.4	0.93	0.31	0.31	0.31[a]		*X*
C-21	aluminum *Z* panel	0.31	rigid polyurethane foam	4.0	21.1	0.93	0.31	0.31	0.31[a]		*X*
T-2	aluminum 2024T3	0.32	rigid polyurethane foam	6.38	19.1	1.06	0.32	0.74	...	*X*	
G-1	Dacron-Butyl	0.42	flexible latex foam	6.0	16.5	1.20	0.42	0.78	...	*X*	
G-3	Dacron-Butyl	0.42	flexible latex foam	6.0	19.5	1.20	0.42	0.78	...	*X*	

[a] Interior wall weight included because of pitting.

The cavity shape thus was shown empirically by means of the experiments to depend on the effectiveness of the bumper in fragmenting the impacting particles which have been shown experimentally to be dependent on the projectile speed and material, and bumper mass.

Mechanical Atmosphere Protection Concept

Bumper and spacer damage constitute one criterion for evaluating the penetration resistance of impacted constructions, but total weight of penetration into the specimen is considerably more important. A quantitative comparison of penetration resistance for specimens of different designs is obtained by computing the weight per unit area of the specimen to the depth of the penetration.

Table 1 presents a summary of the penetrated weight of all target specimens by Pyrex projectiles of approximately equal velocities (20,000 fps). The specimens are listed in descending order of resistance—that having the greatest total penetrated weight, which, in ballistics technology, refers to the area density (oz/ft²) to which visible damage was incurred. The total penetrated weight of the specimens seems to decrease with decreased bumper and spacer mass.

The interior wall usually sustained no visible damage, although at times it prevented penetration into various specimens. This effect tends to obscure quantitative evaluation of impact damage. Further experimentation is needed before the effectiveness of the inner wall in stopping penetration can be accurately evaluated.

Figure 8 is a plot of penetrated foam weight vs foam density for instances in which penetration was arrested in the spacer medium. Specimen *D*-17 is not included because of the relative ineffectiveness of the *Z*-panel bumper. Specimens *G*-1 and *G*-3 are excluded because the foam medium used was not polyurethane. Specimens *T*-2 and *U*-1 are shown in Fig. 9.

Several very interesting trends and conclusions can be drawn from Fig. 8. Specimens *U*-1, *E*-7, *E*-9, and *T*-1 all have approximately equivalent 2024T3 aluminum bumper masses with different densities of rigid polyurethane foam. The weight of the foam, to the penetration depth, decreases with decreased foam density. This observation also can be derived from Table 1.

The observed straight line is actually an equation derived in the following manner. The maximum penetration depth observed was experimentally obtained, and its development will be discussed in a later paragraph.

$$\rho(L - 1.27) = 0.416 \tag{2}$$

where ρ is the foam density (lb/ft³) and L the maximum foam penetration depth (in.). Rearranging,

$$L = 1.27 + (0.416/\rho) \tag{3}$$

Multiplying both sides by $\rho/12$ the penetrated surface weight in pounds per square foot is obtained:

$$(L\rho/12) = 0.106\rho + 0.0347 \tag{4}$$

If specimens *K*-1 and *K*-2 are added to the polyurethane foam penetration-weight curve, they will fall very close to the established line. Specimens *K*-1 and *K*-2 are constructed of a flexible polyurethane foam spacer and of a fiberglass-silicone bumper. Their weights are approximately 45% of the other specimens shown.

Total penetrated weight vs foam density is shown in Fig. 10, which presents two additional test points. Specimen *H*-5 represents an equivalent *K* specimen with the exception that the bumper was of 2024T3 aluminum. Specimen *J*-2 also is equivalent to *H* or *K*, except that no bumper wall was used. Both *H*-5 and *J*-2 should have greater total penetrated weight, since penetration was stopped by the inner wall. Arrows on the curve indicate this condition.

Several conclusions can be drawn from Fig. 10: 1) the lower the foam density becomes, the greater its penetration resistance per unit weight; 2) fiberglass fabric is more effective as a bumper than an aluminum wall of equal weight; and 3) a decrease in bumper weight causes a decrease in the total penetrated weight. Conclusion 3 comes from the fact that bumper specimens *K*-1 and *K*-2 weigh 45% less than those indicated by the straight line. The implication that no

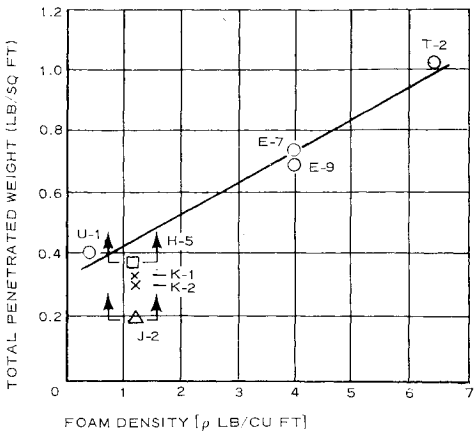

Fig. 10 Total penetrated weight comparison.

bumper is best cannot be confirmed or denied until the exact position of *J*-2 is known. Although it must be emphasized that these conclusions are based on experimental results of certain projectile materials and speeds, they nevertheless merit extensive investigation and study.

Reliable formulas for calculating the single-sheet thickness required to stop a given projectile were generally developed for metals and have been experimentally verified to approximately 20,000 fps. The most commonly used formula, developed by NASA Ames,[7] is

$$t = 3.42 d_P \left(\frac{\rho_p}{\rho_t} \cdot \frac{V}{C}\right)^{2/3} \tag{5}$$

where

t = plate thickness necessary to stop a given projectile
d_P = projectile diameter
ρ_p = projectile density
ρ_t = target density
V = projectile velocity
C = velocity of sound in target

As shown in Fig. 11, specimen *J*-2, a spacer of flexible 1.2 lb/ft^3, polyurethane foam of 2-in. thickness weighing 0.20 psf was able to stop a 21,900 fps, 0.063-in. diam, 4.54 mg Pyrex projectile having a density of 2.12 g/cm^3, without visible damage to the structural wall. On the other hand, a single sheet of aluminum weighing 3.14 psf would be required, as found by the foregoing formula, to stop an identical projectile traveling at the same velocity. The comparison of 0.20 and 3.14 psf shows an increase in efficiency of penetration resistance for foam by an efficiency factor of 15.7 to that of a single-wall aluminum structure. Other foam designs could have much greater resistance to penetration.

This ability of foam to absorb and arrest an impacting projectile appears somewhat analogous to the atmospheric dissipation of meteors. The basic system of protection from hypervelocity particle impacts by using foam as the essential component, therefore, is identified by Goodyear Aerospace Corporation as a mechanical-atmosphere protection system, whose efficiency factor is expected to increase with impacting velocity increase. The expected increase in efficiency factor is important, since meteoroid impacts for the most part are expected to be above 50,000 fps.

Experimental work with particle velocities to 22,500 fps showed that the efficiency of the protection system decreased as the impacting particle velocity decreased and as the impacting particle density increased. The decrease in efficiency from these causes is relatively unimportant for a near-earth environment, since the average velocities of meteoroids are above 50,000 fps and since massive, steel-like particles are very infrequent.

The use of foams in space structures requires consideration of other factors, such as vibration and shock. The data obtained from vibration and shock tests conducted on 6-in. cubes of rigid polyurethane foam is tabulated in Table 2. None of these specimens showed any tendency to disintegrate when severely shock-tested by blows from a heavy hammer, except for the rigid foam with a density of 1.5 lb/ft^3 that fractured very easily under a slight shock imposed by hand. The test results indicate that flexible foams should be used if foam densities of 1.5 lb/ft^3 or less are required in a structure subject to vibration and shock loads.

Skin thickness limitations are often encountered in vehicle designs. The penetration depth of a specimen thus assumes increased significance. The curve of penetrated foam length vs foam density is presented in Fig. 12. At zero foam density the penetrated foam length would be expected to be infinite. At the higher foam densities, above 4 lb/ft^3, the penetrated length remained approximately constant. A hyperbola of the form $x(y - \alpha) = \beta$ was then empirically fitted and an equation obtained having a standard deviation of 7.6%

$$\rho(L - 1.27) = 0.416 \tag{6}$$

The use of a mechanical atmosphere leads to a re-evaluation of the purpose of a bumper wall. An outer wall is required

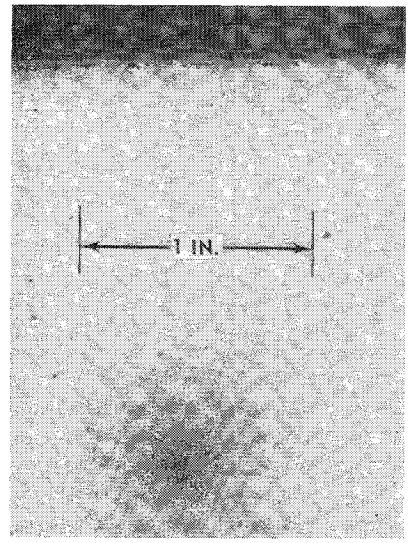

Projectile, 0.0063-in. Pyrex; velocity, 21,900 fps; spacer, 1.2 lb/ft^3 flexible polyurethane foam

Impact surface, specimen *J*-2

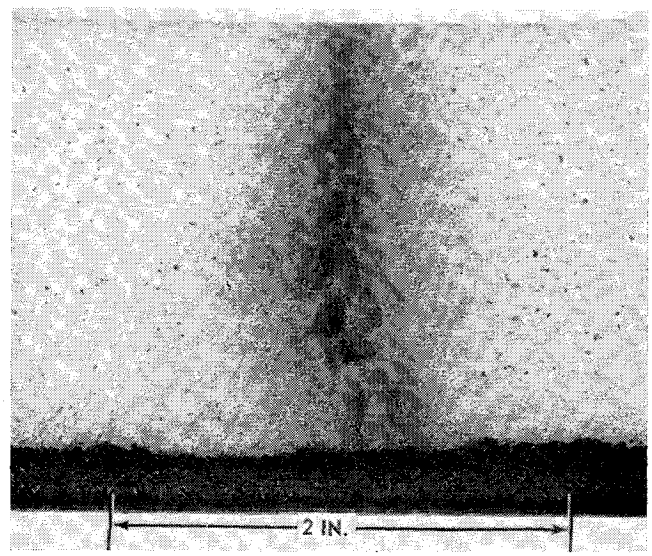

Cross section, specimen *J*-2

Fig. 11 Mechanical atmosphere concept.

Table 2 Rigid foam vibration and shock test data

Density, lb/ft³	Input, g	Resonance frequency, cps	Output, g	Test time at resonance, min
6.0	25	500	350	5
4.0	25	500	300	5
2.5	25	490	380	5
1.5	25	470	485	5

in a space structure using the mechanical-atmosphere protection system: to protect the foam during handling, ascent, and deployment operations, to shield the foam from the effects of ultraviolet radiation, and to maintain proper absorptive and emissive characteristics for thermal control.

Conclusions

Optimization of the mechanical atmosphere system of protection from meteoroid impacts is being investigated in keeping with the considerable promise of polymeric and foamed materials revealed by the hypervelocity terminal effects. The following information was learned from initial investigations:

1) Without a bumper, the foam spacer penetration resistance to Pyrex projectile velocities over 21,900 fps was comparable to or better than the resistance of equal-weight aluminum structures. The foam spacer exhibited an efficiency by weight 15.7 times that of a single aluminum wall.

2) Both rigid and flexible foam spacers, as mechanical atmospheres, tend to absorb and arrest impacting materials through vaporization.

3) When foam spacers were absent, aluminum structural walls sustained greater damage than equivalent weight fabric walls against 20,000 fps Pyrex projectiles.

4) An aluminum sheet bumper is superior to an equal weight Z panel of crushed aluminum honeycomb against 20,000 fps Pyrex projectiles.

5) A fiberglass-silicone bumper is superior to an equal weight Z panel of crushed aluminum honeycomb against 20,000 fps Pyrex projectiles.

6) Failures about the impact holes for some materials indicate that bumpers should be made of homogeneous materials or of high-temperature composites.

7) The use of a bumper for fragmenting hypervelocity particles requires re-evaluation if foam is used as a spacer.

The specimen design for meteoroid protection of a manned space structure is shown in Fig. 13. The bumper serves as a protective layer for handling purposes and other abrasive conditions. It also serves as an optical coating for thermal balance when in space. Only incidentally does the bumper tend to fragment impacting hypervelocity particles. The foam spacer absorbs, arrests, and/or vaporizes the impacting materials; the foam spacer also positions the bumper from the structural wall. The structural wall resists penetration

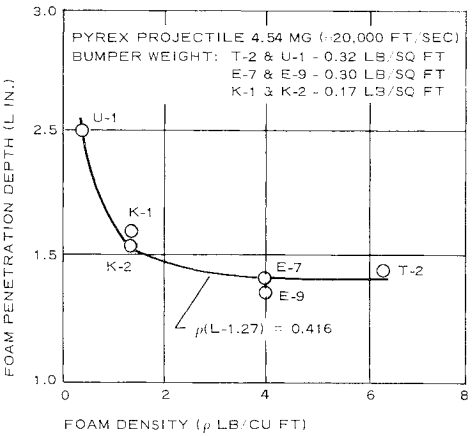

Fig. 12 Foam penetration depth.

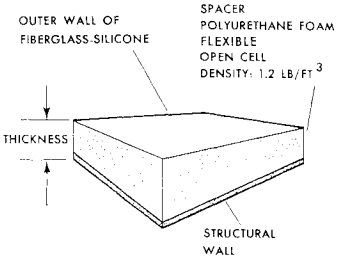

Fig. 13 Protection concept for manned space structures from meteoroid penetration.

by particles not already degraded to negligible levels. However, the structural wall primarily carries the structural loads and serves as the gas-retaining wall for pressurized, manned, space structures.

References

[1] Thompson, A. B. and Gell, G. F., "Meteoroids as a hazard in space flight—a survey of present information," ARS Preprint 2138-61 (October 9–15, 1961).

[2] Reynolds, B. W., "Effects of hypervelocity particle impact on composite materials for expandable structures applications," GER-10663, Goodyear Aerospace Corp., Akron, Ohio, (August 1962).

[3] Whipple, F. L., "Dust and meteorites," Astronautics **7,** 40–42 (August 1962).

[4] Davidson, J. R. and Sandorff, P. E., "Environmental problems of space flight structures part I, meteoroid hazard," preliminary draft (March 1962).

[5] Whipple, F. L., "The meteoritic risk to space vehicles," *Vistas in Astronautics* (First Annual Air Force Off. Sci. Res. Astronautic Symp., 1958).

[6] Funkhouser, J. O., "Preliminary investigation of the effect of bumpers as a means of reducing projectile penetration," NASA TN-D 802 (April 1961).

[7] Nysmith, C. R. and Summers, J. L., "Preliminary investigation of impact on multiple sheet structures and an evaluation of the meteoroid hazard to space vehicles," NASA TN-D-1039 (September 1961).